Dynamics of El Niño Southern Oscillation

Nabil Swedan (nabilswedan@yahoo.com)
Pacific Engineering PLLC, Redmond, WA

Research Article

Keywords: El Niño, Oceanic Niño Index, Ocean, Atmosphere, Thermodynamics, Theoretical Model

Posted Date: November 10th, 2023

DOI: https://doi.org/10.21203/rs.3.rs-1322232/v2

Additional Declarations: No competing interests reported.

Abstract

The hazards associated with El Niño Southern Oscillation (ENSO) are documented in the literature. They include but are not limited to droughts, floods, extreme temperatures, and tropical cyclone count cycles. It appears that during ENSO warming phases, the number of typhoons increases and the number of hurricanes decreases. The opposite occurs during cold phases. The present ENSO understanding assumes that the oscillation is self driven indefinitely, which is thermodynamically unfeasible. Energy supply is required. Furthermore, features of the observed Oceanic Niño Index have remained uncaptured by ENSO models, and long-term prediction of El Niño has remained a challenge. This work reveals that the observed uneven surface warming between the hemispheres induces heat cycles in the hydrosphere, the outcome of which is El Niño events. During an event, tropical winds are practically arrested, and wind thrust and momentum fluxes produce potential energy cycles of the tropical air mass. Fluctuation of the potential energy exchanges heat with sea water in El Niño region and warm and cold episodes of ENSO manifest. Accordingly, the theoretical equation of the Oceanic NiñoIndex is derived. It is compared with observations and an agreement appears to exist. The equation is then used to calculate and project the index between 2015 and 2024. Because the uneven warming between the hemispheres is increasing, the frequency of El Niño events is expected to increase.

1. Introduction

Caviedes (2001) provides a description of El Niño events, how and where they occur, their impact on the economy, as well as their imprint on world history. El Niño phenomenon is a major event that can adversely affect the livelihoods of many regions of the world. El Niño events occur towards the end of the year, during the southern hemispheric summer in the tropics west of South America. The energy associated with the event is large, on the order of all tropical typhoons combined. It is large enough to split the earth into two hemispheres, east and west with climate “teleconnections.” Severe weather extremes including but are not limited to heavy rainfall, strong winds, droughts, and extreme temperatures are typically associated with El Niño and the resulting El Niño Southern oscillation (ENSO). The duration and frequency of the observed floods in South East Asia and the world over appear to be correlated with ENSO (Ward et al. 2016). The tropical cyclone count cycles with ENSO. Koltzbach (2011) summarizes the work of researchers relative to the historical record of hurricane landfalls on the U.S.A. The conclusion is that the number of hurricanes increases during La Niña and decreases during El Niño phases of ENSO. The author, in the published paper (Swedan 2020), analyses the observed hurricane and typhoon counts for the period of time between 1981 and 2005*. “Hurricane and typhoon counts appear to exhibit opposite count cycles: if the number of typhoons increases, the number of hurricanes decreases and vice versa.”* Therefore, there is general conclusion that may be deduced based on the record of tropical cyclones: During El Niño episodes, the number of typhoons increases and the number of hurricanes decreases. During La Niña episodes, it is the opposite. The number of typhoons decreases and the number of hurricanes increases. Clearly, El Niño events and the subsequent El Niño and La Niña phases potentially

pose serious hazards. An understanding of ENSO physics and dynamics may thus be beneficial for research and society.

Wang et al. (2016) and Wang (2018) present overviews of the scientific evolution of ENSO understanding, ENSO mechanisms, and the related hypotheses and theories, and provide a large number of references for further reading on the subject. Although ENSO has become increasingly known to the scientific community, more research in this field is recommended by these overviews. ENSO is assumed to be a product of self-sustained oscillators that work together to alter thermocline depth anomalies and maintain ENSO steady. The oscillators are products of ocean-atmosphere interactions with negative feedbacks from the ocean and atmosphere that sustain the oscillation indefinitely. An and Jin (2004) indicate that this ENSO scientific understanding does not explain the nonlinear nature of ENSO. In Figs. 1 and 2, the observed value of the Oceanic Niño Index (ONI) is presented in red solid lines. The index measures sea temperature anomalies in Niño region 3.4, located at the equator between 5°N-5°S and 120°W-170°W, please see the data section for more details. The index appears to have carried over -0.5 °C from the earlier oscillation. When this is accounted for, the amplitude of the index is damped with time, and the warm phases have larger amplitudes than the cold phases. In addition, self sustaining oscillators are not thermodynamically possible, energy supply is required. Although climate models simulate the observed sea temperature anomalies well, they do not appear to capture the observed asymmetry in sea temperature anomalies (Hayashi et al. 2020), or predict El Niño events more than six month before their occurrence. Clearly, the physics of ENSO does not appear to be fully understood, and as a result, a long-term prediction of the associated risks and hazards does not appear to be possible at this time.

This work indicates that the observed uneven warming between the hemispheres (CRU 2023) have produced heat cycles in the hydrosphere (Swedan 2020) in the form of warm water. The global rise in sea temperature induces a warm water anomaly in the tropics west of South America. When the heat is large enough, tropical winds are weekend considerably during El Niño events. Wind deceleration produces forces and momentum fluxes, and as a result, potential energy cycles of the tropical air mass develop. The potential energy cycles exchange heat with sea water in El Niño region and episodes of warm and cold sea temperatures occur. They continue after El Niño event. To complement the current ENSO understanding, the theoretical equation of ONI, Eq. (20), is derived, and the theoretical ONI is plotted in Fig. 1 for comparison with observations. An agreement appears to exist as discussed in the conclusions section. The equation is then used to calculate and project ONI between 2015 and 2024, Fig. 4.

It should be noted that this manuscript is an integral part of a set of papers, some of which have been already published. Imported texts from these papers are quoted in italics. The manuscript includes theory section in which evolution of El Niño is briefly discussed and the theoretical equation of ONI is derived, data section detailing parameter values used and data sources, sample calculations, error analysis, discussion, and conclusions. For clarity, a Symbols and abbreviations section is provided. The symbols used for this work are explained in the section.

2. Theory and analysis

As discussed in Introduction, the observed ENSO is a damped oscillation. However, because the time between El Niño events has decreased (Li et al. 2011), ENSO appears to be a continuous oscillation. To maintain the oscillation, there has to be an energy supply, it is provided during El Niño events. El Niño is a major thermodynamic process and requires a massive amount of heat for its evolution. The sun provides this heat because the poleward solar heat transport has decreased due to uneven warming between the hemispheres (Swedan 2020). Less solar heat is conveyed poleward, and a heat anomaly in the form of warm water is thus produced in the hydrosphere. Because the global rise in average temperature is least in the tropics, the average sea level expansion is least in the tropics as well. The tropics have, therefore, become low locations, and the warm water gradually accumulates in the tropics with time. It appears that when heat accumulation is large enough, tropical Pacific winds are weakened considerably (Lau and Yang 2015). The sample calculations show that air flow reduces from 1.45×10^{11} kg s^{-1} to 3.85×10^{9} kg s^{-1}, a reduction of nearly 97% in wind flow rate. Simultaneously, the warm water heads east steadily like a slick of oil, as Caviedes (2001) describes the process, and accumulates in El Niño region located in the tropics between ±23.4° and 70°W to 180°E, data section. The warm water provides a heat supply to El Niño throughout its entire duration. In this work, the heat supply is referred to as El Niño heat, Q_{sn}, calculated in the sample calculations section to be nearly equal to 7.05×10^{21} J.

Referring to Fig. 3, the horizontal velocity of surface winds, v_h, is nearly arrested during El Niño, Fig. 3b, and, therefore, the vertical components of atmospheric air flow and forces are relevant for the objectives of this work. Before El Niño, Fig. 3a, the upward air mass flow rate, M, is assumed to be at steady state having vertical velocity v. Air flow and velocity decrease substantially during El Niño to M_n and v_n respectively, Fig. 3b. Caballero (2014) and Fleagle and Businger (1980) discuss atmospheric air related properties, physics, thermodynamics, forces, and equations of motion. Accordingly, for the volume of air in El Niño region that is enclosed by the dashed lines of Figs. 3a and 3b, the resultant of atmospheric force may include buoyant upward force, Coriolis force, and variation in air mass momentum flux through volume boundary. The latter induces reaction force or thrust on the air volume. Before an El Niño event, the component of the resultant of atmospheric forces in Z direction, or vertical to the surface, may be written as follows:

$$F_z=F_b+F_{cz}+(dm_e/dt)\, v_e-(dm_o/dt)\, v_o \qquad (1)$$

Where

F_z=Component of the resultant of atmospheric forces in Z direction, N.

F_b=Buoyant upward force, N.

F_{cz}=Component of Coriolis force in Z direction, N.

m_e=Mass of the air entering the air volume enclosed by the dashed lines, kg.

v_e =Velocity of the air entering the air volume, m s^{-1}.

m_o=Mass of the air exiting the air volume, kg.

v_o =Velocity of the air exiting the air volume, m s^{-1}.

t =Time, s

In Eq. (1), friction forces in Z direction are not considered because air streams move upward, away from the surface, and velocity gradients between the air streams may be neglected. The difference $(dm_e/dt)\ v_e$-$(dm_o/dt)\ v_o$ is equal to the force or thrust imparted by air flow streams in and out of the air volume enclosed by the dashed lines of Fig. 3. This difference is equal to d(m v)/dt, where m is the mass of the air volume, kg, and v is air volume velocity, m s^{-1}. Equation (1) simplifies

$$F_z=F_b+F_{cz}+d(m\ v)/dt \qquad (2)$$

Where

d(m v)/dt=Variation in the flux of air mass momentum with time, N.

m =Mass of air in the volume enclosed by the dashed lines of Fig. 3 in El Niño region, kg.

v =Velocity of the air mass, m s^{-1}.

Although the warm mass of air in El Niño region is large and straddles the equator, it is only 4% or less of the total mass of the surrounding colder atmospheric air. Therefore, the force of buoyancy may be expressed as follows:

$$F_b=(\delta-\delta_n)\ A_n\ Z_T\ g \qquad (3)$$

Where

δ =Average density of the surrounding air, kg m^{-3}.

δ_n =Average air density in El Niño region, kg m^{-3}.

A_n =Area of El Niño region, m^2.

Z_T =Height of tropical tropopause, m.

g =Gravity acceleration, m s^{-2}.

The component of the Coriolis force in Z direction, F_{cz}, may be obtained from the total force of Coriolis

$$\mathbf{F_c} = -2\ m\ \boldsymbol{\omega} \times \mathbf{v_r} - 2\ m\ \boldsymbol{\omega} \times \mathbf{dZ(t)/dt} \quad (4)$$

Where

$\mathbf{F_c}$=Total force of Coriolis, N.

$\boldsymbol{\omega}$=Angular velocity of the earth around its axis, radians s^{-1}.

$\mathbf{v_r}$= Relative horizontal velocity between the air mass in El Niño region and surface, m s^{-1}.

dZ(t)/dt= Relative velocity between the air mass in El Niño region and the surface, m s^{-1},

represented by the variation in the height of the air mass.

The symbols in bold font of Eq. (4) indicate vectors and their cross products. During El Niño, there is no tangible horizontal movement of the mass of air m. Therefore, air mass relative velocity with respect to the surface, $\mathbf{v_r}$, may be neglected. The first term on the right side of Eq. (4), -2 m $\boldsymbol{\omega}$ x $\mathbf{v_r}$, may thus be discarded. The second term of the equation, -2 m $\boldsymbol{\omega}$ x **dZ(t)/dt**, is always perpendicular to Z and can have no component in Z direction. The term F_{cz} of Eq. (2) may be omitted as well. At steady state before El Niño event, the net atmospheric force and its components are nearly equal to zero. Therefore, v is about constant ($dv/dt \approx 0$), and the term d(m v)/dt of Eq. (2) simplifies

$$d(m\ v)/dt = v\ dm/dt + m\ dv/dt = v\ dm/dt \quad (5)$$

At steady state before El Niño event $F_z \approx 0$, and equations 2, 3, and 5 give

$$0=(\delta-\delta_n)\ A_n\ Z_T\ g+v\ dm/dt \qquad (6)$$

At steady state during El Niño event, $F_z \approx 0$ and equations 2, 3, and 5 give

$$0=(\delta-\delta_n)\ A_n\ Z_{Tn}\ g+ v_n\ dm/dt \qquad (7)$$

Where

Z_{Tn} =Height of tropical tropopause during El Niño event, m.

v_n =Vertical air velocity during El Niño event, m s^{-1}.

The right sides of equations (6) and (7) are similar to the right side of Eq. (2). The difference between them is thus equal to variation in atmospheric force, F_z, when air flow decelerates from M at steady state to M_n during El Niño event, Fig. 3. Therefore

$$-dF_z=(\delta-\delta_n)\ A_n\ Z_{Tn}\ g + v_n\ dm/dt-(\delta-\delta_n)\ A_n\ Z_T\ g-v\ dm/dt \qquad (8)$$

The term $-dF_z$ on the left side of Eq. (8) is equal to $-d(m\ d^2Z/dt^2)=-(dm/dt)\ d^2Z/dt^2 \times dt-m\ d^3Z/dt^3 \times dt$. If air deceleration, $-d^2Z/dt^2$, is assumed to be about constant with time, then $-d^3Z/dt^3 \approx 0$ and $-dF_z \approx -(dm/dt)\ d^2Z/dt^2\ dt$. The term (dm/dt) of this equation represents the increase in air mass above El Niño region that is required to remove El Niño heat from sea water. It is equal to the air mass flow rate M_n as required by the air mass balance of the volume enclosed by the dashed lines of Fig. (3b). Therefore, $-dF_z \approx -M_n\ d^2Z/dt^2\ dt$. If the period of time, dt, is selected to be equal to the time required for one complete El Niño event, or one year as will be discussed later in this section, Eq. (8) yields the following relationship:

$$-M_n\, d^2Z(t)/dt^2=(\delta-\delta_n)\, A_n\, (Z_{Tn}-Z_T)\, g + dm/dt\, (v_n-v) \quad (9)$$

Where

M_n=Annual air mass flow rate during El Niño, kg yr^{-1}.

The difference, $(Z_{Tn}-Z_T)$, represents variation in the height, ξ(t), of the tropopause or air mass above sea water in El Niño region. The difference (v_n-v) is equal to dξ(t)/dt. Consequently, Eq. (9) gives

$$M_n\, d^2\xi(t)/dt^2+(dm/dt)\, d\xi(t)/dt+(\delta-\delta_n)\, A_n\, g\, \xi(t)=0 \quad (10)$$

Where

ξ(t)=Variation in the height of tropical tropopause or air mass in El Niño region, m.

Equation (10) is a differential equation of the second order. Its solution contains two arbitrary constants at initial conditions; specifically, initial phase angle and initial amplitude. These conditions may be obtained from the observed Oceanic Niño Index. For comparison with the observed Oceanic Niño Index, Fig. 1 lines in solid red color, the initial phase angle may be assumed to be equal to zero at time t=0. In Fig. 2, the observed index for the months of November, December, and January when El Niño events occurs is plotted. The figure shows that nearly one year (1997 to 1998 and 2015 to 2016) is required to remove the solar heat during EL Niño events. This may not be a coincidence: Just like seasonal variation, El Niño events appear to require one year to remove the entire solar heat anomaly from sea water. Thermodynamics of the earth is a repeatable process, every year. Seasonal variation and El Niño are thermodynamic transformations displaced differentially from equilibrium. Based on the present state of thermodynamic understanding (Lin et al., 1984), they may be considered as reversible transformations. Therefore, the sum of variation in surface heat and variation in energy of the atmosphere is equal to zero at the completion of a full revolution of the earth around the sun. This is a thermodynamic requirement of the earth system dictated by astronomical parameters, which agrees with basic observations. As a result, the time required to complete an El Niño event may be assumed to be

equal to one year. Based on this discussion and Fig. 2, at time t=1 yr, the phase angle is equal to 90°, and $\xi(t)=\xi_0$ and

$$\xi(t)=\xi_0 \text{ Exp}[-(dm/dt)\ t/2M_n] \text{ x sin } [t\{(\delta-\delta_n)\ A_n\ g/M_n-\{(dm/dt)/2M_n\}^2\}^{0.5}] \quad (11)$$

$$\xi(t)/\xi_0= \text{Exp}[-(dm/dt)\ t/2M_n] \text{ x sin } [t\{(\delta-\delta_n)\ A_n\ g/M_n-\{(dm/dt)/2M_n\}^2\}^{0.5}] \quad (12)$$

Where

ξ_0 =Initial amplitude of the air mass oscillation in El Niño region, m.

$\xi(t)$ =Instantaneous amplitude of the air mass oscillation, m.

On the other hand, variation in the height of the air mass dZ(t) and variation in surface heat are correlated. When an air parcel having unit mass gains heat, dQ_a, from the surface, the air internal energy and potential energy increase in accordance with the first law of thermodynamics (Lin et al., 1984):

$$dQ_a=dU+dW \quad (13)$$

$$-dQ_s=dQ_a \quad (14)$$

Where

dQ_a=Heat gained by unit air mass, J kg^{-1}.

dU=Internal energy gained by unit air mass, J kg^{-1}.

dW=Work (potential energy) produced by unit air mass, J kg^{-1}.

dQ_s=Heat lost by the surface per unit air mass, J kg^{-1}.

$$-dQ_s= dQ_a=dU+g\ dZ(t)/2 \quad (15)$$

The division of dZ(t) by 2 in Eq. (15) is required because the potential energy must be calculated at average variation in the height of the air mass. Because heat exchange with the atmosphere is a frictionless thermodynamic process that occurs slowly with time, equipartition of energy is the result, and dU=g dZ(t)/2. Therefore, Eq. (15) gives $-dQ_s=2\ g\ dZ(t)/2=g\ dZ(t)$. Or, variation in the potential energy of atmospheric air mass is equal to the opposite sign of variation in surface heat. This correlation may be used to convert fluctuation in the height of the air mass $\xi(t)=dZ(t)$ of Eq. (11) into variation in surface heat as follows:

$$Q_s(t)=Q_{sn} \times \xi(t)/\xi_0 \qquad (16)$$

Where

$Q_s(t)$=Instantaneous variation in heat content of sea water in El Niño region, J.

Q_{sn}=El Niño heat, or initial sea water heat anomaly, J yr^{-1}.

The fluctuations of the instantaneous heat, $Q_s(t)$, produces ENSO warming and cooling episodes in El Niño region, damped with time, long after the entire El Niño heat Q_{sn} has been removed from sea water. To calculate sea temperature variation of these episodes, the following heat and mass balance may be used:

$$\Delta T_{sn} = Q_s(t)/[M\ C_p] \qquad (17)$$

$$E = M\ (W_s - W_t) \qquad (18)$$

Where

ΔT_{sn} =Variation in average sea surface temperature of El Niño region, which is equal to variation in sea surface air temperature in the region, °C.

M =Annual average surface air flow rate in El Niño region, kg yr^{-1}.

C_p =Air specific heat, J kg^{-1} $°C^{-1}$.

E =Annual average evaporation in El Niño region, kg yr^{-1}.

W_s =Air humidity at saturation with tropical sea water, kg water per kg dry air, dimensionless.

W_t =Air humidity at the tropopause, 0.0 kg water per kg dry air, dimensionless.

The value of ΔT_{sn} is an average sea temperature anomaly of the entire El Niño region. At the equator where Niño region 3.4 is defined, sea surface temperature observes maximum anomaly, which may be assumed to be equal to $2\Delta T_{sn}$. The temperature anomaly in Niño region 3.4, $2\Delta T_{sn}$, is by definition equal to the Oceanic Niño Index. By eliminating M from equations (17), the instantaneous index value may be presented as follows:

$$\text{Instantaneous Oceanic Niño Index (ONI)} = 2 \times Q_{sn} \times [\xi(t)/\xi_0] \times W_s/(E\, C_p) \quad (19)$$

Multiplying the right side of Eq. (19) by 2/π, the average value of the index follows:

$$\text{Average ONI} = (4/\pi) \times Q_{sn} \times [\xi(t)/\xi_0] \times W_s/(E\, C_p) \quad (20)$$

3. Data

El Niño Southern Oscillation is monitored by a number of El Niño indexes, some of which are described in Trenberth and Hoar (1996) and Trenberth et al. (2002). Generally, an index measures sea temperature fluctuation in a defined region in the tropics west of South America with respect to a base period of time. For the Oceanic Niño Index considered for comparison with the work presented in this manuscript, El Niño region 3.4 is the defined region, located between 5°N-5°S and 120°W-170°W). It is located at the equator and observes nearly maximum temperature anomalies. The National Oceanic and Atmospheric Administration (NOAA 2023) and the National Center for Atmospheric Research (NCAR 2023) present calculation methodology and observed values of the index. Index values within ±0.5 °C are considered Niño neutral. Below this value, a cooling phase or episode typically referred to as Niña manifests. Values above 0.5 °C are referred to as Niño or warming phase or episode. This, however, is to be distinguished from an El Niño event during which massive amount of energy is exchanged with the surroundings. The events are characterized by maximum amplitude of the index, nearly 2.5 °C, Fig. 2, which shows two events, in 1996/1997 and 2014/2015.

The physical parameters of the ocean and atmosphere prior and during an El Niño event should be defined. These parameters dictate the values of the terms of the equations derived in the theory section. Fleagle and Businger (1980) present the U.S. standard atmosphere. At nearly 20 kPa, the global average height of tropopause Z_T is 1.2 x 10^4 m. For the tropics at 28 °C (NOAA, 2022), Z_T is thus approximately equal to 1.25 x 10^4 m. The U.S. standard atmosphere gives global average air density, δ, at 50 kpa of nearly 0.691 kg m^{-3}. Therefore, at the tropics the average air density, δ_n, is about 0.633 kg m^{-3}. Required for application of the derived equations are values of evaporation and air humidity at sea water saturation temperature in the tropics. Gruber and Levizzani (2008) estimated average global precipitation to be about 2.61±0.23 mm day^{-1} (relative error of ±0.09), which is equal to global evaporation. However, at the regional level evaporation is not necessarily equal to precipitation. In the tropics, evaporation must be greater than precipitation, for much of tropical moisture travels to higher latitudes. Meteorological records and evaporation data do not appear to be available for El Niño region at this time. A comprehensive analysis of evaporation study in Peru using a piche evaporimeter was prepared by Chanduvi-acña (1969). Based on this reference, weather stations having elevation near sea level and highest average temperature of 22.78 °C recorded an annual average evaporation of 4.93 mm d^{-1}. Application of equation (21) of Swedan (2018) at average temperature of 22.78 °C gives annual average evaporation of 4.30 mm d^{-1}. Because the annual average sea temperature in El Niño region is greater than 22.78 °C, nearly 28 °C, the equation yields 6.08 mm d^{-1} for evaporation, which will be used for El Niño region. Evaporation error is nearly ±0.09. The psychrometric chart (Goldberg 1996) gives air humidity of 0.0238 kg water per kg dry air at saturation temperature of 28 °C and air specific heat C_P=1 000 J kg^{-1} $°C^{-1}$.

Important physical parameters are solar heat of El Niño and area of El Niño region. Trenberth et al. (2002) discuss spatial and temporal evolution of El Niño. As Fig. 13 of this reference and its related discussion indicate, statistically significant El Niño warming may be assumed to cover nearly 70% to 80% of the surface area between the tropics (±23.4°) and 70°W to 180°E. Therefore, El Niño region has a surface area A_n of nearly 4.91 x 10^{13} m^2. The value of El Niño heat, Q_{sn}, is required, and a summary of its sample calculations is tabulated in Table 1. The value of Q_{sn}, is approximately equal to 7.05 x 10^{21} J.

4. Sample calculations

Parameterization of energy cycles methodology as explained by Swedan (2020) may be utilized to calculate climate heat exchange between the hemispheres. From equations (1), (2), (3), and sample calculations of this reference, the heat calculation is quoted as follows:

$$\text{“}\Delta h_f = \beta\, d_m\, (T_{SH}-T_{NH}) \qquad (21)$$

$$\Delta Q_n = -[\{(0.2+\Delta h_f)/0.2\}^{0.5}-1] \times Q_{PHT} \qquad (22)$$

Where

h_f *=Available average liquid elevation for the thermohaline brine flow, 0.2 m.*

β *=Sea water volumetric thermal expansion, 200 x* 10^{-6} *°C*$^{-1}$*.*

d_m *=Average depth of ocean mixed layers, 95 m.*

T_{SH} *=Average annual sea temperature of the southern hemisphere, °C.*

T_{NH} *=Average annual sea temperature of the northern hemisphere, °C.*

ΔQ_n *=Calculated annual climate cycle heat exchanged between the hemispheres, J* yr^{-1}*.*

Q_{PHT}*=Poleward heat transport, 5.52 x*10^{22} *J* yr^{-1}*.*

The quantity Δh_f *is equal to variation in liquid elevation available for the thermohaline brine flow at surface water with sea temperature difference between the hemispheres. The term* $(0.2+\Delta h_f)/0.2$ *is equal to the ratio between variation in the available liquid elevation and that of average liquid elevation of the thermohaline brine flow of 0.2 m. The term* $[\{(0.2+\Delta h_f)/0.2\}^{0.5}-1]$ *is equal to the ratio between variation in flow of the thermohaline brine and its average flow value, assumed as river flow or fluid flow in channels. Also, this ratio is equal to the ratio between variation in heat flow of warm water conveyed by the thermohaline circulation and its average heat flow. The value of average heat flow is equal to the poleward heat transport,* Q_{PHT}*, of 5.52 x* 10^{22} *J* yr^{-1}*. Therefore, Eq. (22) gives annual heat exchanged between the hemispheres resulting from the difference in sea temperature between the hemispheres. The negative sign of right side of Eq. 22 is a convention to indicate heat deficit of the northern hemisphere."*
The cumulative value of the annual heat ΔQ_n between two consecutive El Niño events is equal to El Niño heat Q_{sn}. In Table 1 the value of Q_{sn} is calculated for the period of time between the events that occurred in 1997 and 2015. The difference in sea temperature between the hemispheres is provided by CRU (2023). They are given as sea temperature anomalies for the northern and southern hemispheres. The difference between them is equal to $(T_{SH}-T_{NH})$ required for Eq. (22). For the year 1998, $(T_{SH}-T_{NH})=-0.061$ and $\Delta Q_{1988} = -[\{(0.2+200 \times 10^{-6} \times 95 \times 0.061)/0.2\}^{0.5}-1] \times 5.52 \times 10^{22}=1.60 \times 10^{20}$ J. The calculation is repeated every year through 2015, and the cumulative value of ΔQ_n is approximately equal to $Q_{sn}=7.05 \times 10^{21}$ J. This is the amount of solar heat anomaly required for El Niño.

Required for the application of Eq. (20) is the value of dm/dt, which is part of the decay factor of the oscillation $(dm/dt)/2M_n$. The value of dm/dt is a constant, dictated by astronomical parameters and represents variation in the mass of atmospheric air for any given latitude in one year. If the mass of air is

imagined to have a uniform temperature and density, δ, at all latitudes then dm/dt=0 for every latitude. However, air at lower latitudes is warmer and more buoyant than the surrounding air located at higher latitudes, and air mass infiltration from the surroundings is expected. Therefore, dm/dt≠0, and the value of dm/dt may be estimated for all latitudes in general and El Niño region in particular as follows: The value of dm/dt is equal to the variation in air mass of the volume enclosed by the dashed lines of Fig. (3b) in one year, during which air having density that is equal to δ_n is replaced by the surrounding air having density that is equal to δ

$$dm/dt \approx \Delta m/\Delta t=(\delta V-\delta_n V)/t \quad (23)$$

$$dm/dt \approx [(\delta-\delta_n)\ A_n\ Z_T\ ]/\tau \quad (24)$$

Where

V=Volume of the air mass above sea water in El Niño region, m^3.

τ=Time of one revolution of the earth around the sun, yr.

Example:

Evaporation caused by El Niño heat, $E_n=Q_{sn}$/Latent heat of water evaporation, $E_n=Q_{sn}/(2.44 \times 10^6)=7.05 \times 10^{21}/(2.44 \times 10^6)=2.89 \times 10^{15}$ kg yr^{-1}. Because gravity acceleration used in the calculations is equal to 9.8 m s^{-2}, all flow rates must be rated per second as well. One year is equal to 3.15×10^7 seconds.

Air flow rate during El Niño, $M_n=E_n/W_s=2.89 \times 10^{15}/(0.0238 \times 3.15 \times 10^7)=3.85 \times 10^9$ kg s^{-1}, Eq. (18).

$dm/dt=(\delta-\delta_n)\ A_n\ Z_T/(3.15 \times 10^7)=(0.691-633) \times 4.91 \times 10^{13} \times 1.25 \times 10^4\ /(3.15 \times 10^7)=1.14 \times 10^9$ kg s^{-1}, Eq. (24).

Argument terms of the sinusoidal function, Eq. (12):

$(\delta-\delta_n)\ A_n\ g/M_n=(0.691-0.633)\ x\ 4.91\ x\ 10^{13}\ x\ 9.8/\ 3.85\ x\ 10^9=7\ 248.95.$

$\{(dm/dt)/2M_n\}^2=\{(1.14\ x\ 10^9)/(2\ x\ 3.85\ x\ 10^9)\}^2=0.02.$

For 1997, t=1 yr.

Oscillation decay factor, $(dm/dt)\ x\ t/2M_n=(1.14\ x\ 10^9)\ x\ 1/(2\ x\ 3.85\ x\ 10^9)=0.148.$

Angle of the sinusoidal function, $[t\ x\ \{(\delta-\delta_n)\ A_n\ g/M_n-\{(dm/dt)/2M_n\}^2\}^{0.5}]=[1\ x\ \{7\ 248.95.-0.02\}^{0.5}]=85.14°$, Eq. (12).

$\xi(1)/\xi_0=Exp\ [-0.148]\ sin\ [85.14]=0.86$, Eq. (12).

$Q_s(1)=Q_{sn}\ x\ \xi(1)/\xi_0=7.05\ x10^{21}\ x\ 0.86=\ 6.06\ x10^{21}\ J\ yr^{-1}$, Eq. (16).

Average annual evaporation in tropics, $E=6.08\ mm\ d^{-1}$, data section.

Average annual evaporation in El Niño region, $E=6.08\ mm\ d^{-1}\ x\ 365\ d\ yr^{-1}\ x\ A_n=6.08\ x\ 365\ x\ 4.91\ x\ 10^{13}=1.09\ x\ 10^{17}\ kg\ yr^{-1}$.

Air mass flow rate in El Niño region, $M=E/W_s=1.09\ x\ 10^{17}/0.0238=4.58\ x\ 10^{18}\ kg\ yr^{-1}\ (1.45\ x\ 10^{11}\ kg\ s^{-1})$, Eq. (18).

Oceanic Niño Index (ONI) for $1997=2\ x\ Q_s(1)\ x\ W_s/[E\ x\ C_p]=\ 2\ x\ 6.06\ x\ 10^{21}x\ 0.0238/(1.09\ x\ 10^{17}\ x\ 1\ 000)=2.65°C$, Eq. (19).

Average Oceanic Niño Index (ONI) for 1997=$4/\pi$ x $Q_s(1)$ x $W_s/[E \times C_p]$= $4/\pi$ x 6.06 x 10^{21}x 0.0238/(1.09 x 10^{17} x 1000)=1.68°C, Eq. (20).

Similar calculations are conducted for the years between 1998 and 2015, and the plot of average ONI is presented in Fig. 1 in blue color.

5. Evaluation of calculation error

For a measured or calculated quantity x, the absolute value of the error is indicated by Δx, and the relative error $\varepsilon x=\Delta x/x$. The maximum absolute error value is Max Δx. The relative error of evaporation, εE, is nearly ±0.09, data section. Because $M_n= E_n/W_s$, Eq. (18), then the relative error εM_n =±0.09. The value of the theoretically calculated poleward heat transport, Q_{PHT}, has an accuracy of ±0.20 (Swedan 2020). Because El Niño heat, Q_{sn}, is a fraction of the poleward heat transport, its relative error εQ_{sn} is ±0.20 as well.

For the argument of sinusoidal function, the symbol θ will be used, and $\theta=t[(\delta-\delta_n)\ A_n\ g/M_n-\{(dm/dt)/2M_n\}^2]^{0.5}$, Eq. (11). Neglecting the second term of the argument based on the sample calculation, then $\theta\approx t[(\delta-\delta_n)\ A_n\ g/M_n]^{0.5}$ and error of θ follows:

$\Delta\theta= 0.5\ t[(\delta-\delta_n)\ A_n\ g/M_n]^{-0.5} \times [(\delta-\delta_n)\ \Delta A_n\ g/M_n-(\delta-\delta_n)\ A_n\ g\ (-\Delta M_n/M_n^2)]$

$\Delta\theta= 0.5\ t[(\delta-\delta_n)\ A_n\ g/M_n]^{-0.5} \times [(\delta-\delta_n)\ A_n\ \varepsilon A_n\ g/M_n+(\delta-\delta_n)\ A_n\ g\ \varepsilon M_n/M_n]$

$\Delta\theta=0.5 \times t[(0.691-0.633) \times 4.91 \times 10^{13} \times 9.8/3.85 \times 10^9]^{-0.5} \times [(0.691-0.633)\ 4.91 \times 10^{13}\ \varepsilon A_n\ 9.8/3.85 \times 10^9+(0.691-0.633)\ 4.91 \times 10^{13} \times 9.8 \times (\pm 0.09)/3.85 \times 10^9]$

$\Delta\theta=0.5 \times t\ [0.0118] \times [7\ 248.95\ \varepsilon A_n \pm 652.41]$

For $\varepsilon A_n=\pm 0.1$, $\Delta\theta=\pm 8.13\ t$.

For t=1 or 1997, $\Delta\theta=\pm 8.13°$.

For t=10 or 2006, $\Delta\theta=\pm 81.30°$.

For t=18 or 2014, $\Delta\theta=\pm 146.37°$.

The calculated error of the Oceanic Niño Index may be analyzed:

$\xi(t)/\xi_0 = \text{Exp}[-(dm/dt)\ t/2M_n] \times \sin[\theta]$, Eq. (12)

$\xi(t)/\xi_0 = \text{Exp}[-1.14 \times 10^9 \times t/(2 \times 3.85 \times 10^9)] = \text{Exp}[-0.148\ t]$

$\text{ONI} = (4/\pi) \times Q_{sn} \times [\xi(t)/\xi_0] \times W_s/(E\ C_p)$, Eq. (20)

The absolute value of the error $\Delta[\xi(t)/\xi_0]$ is negligible.

For $\theta = n \times \pi/2$, the absolute value of the maximum error of ONI follows:

$\text{Max}\ \Delta(\text{ONI}) = (4/\pi) \times \Delta Q_{sn} \times [\xi(t)/\xi_0]\ W_s/(E\ C_p) + (4/\pi) \times Q_{sn} \times [\xi(t)/\xi_0] \times W_s/C_p \times (-\Delta E/E^2)$

$\text{Max}\ \Delta(\text{ONI}) = (4/\pi) \times \Delta Q_{sn} \times (Q_{sn}/Q_{sn})\ [\xi(t)/\xi_0]\ W_s/(E\ C_p) + (4/\pi) \times Q_{sn} \times [\xi(t)/\xi_0] \times W_s/(E\ C_p) \times (-\varepsilon E)$

$\text{Max}\ \Delta(\text{ONI}) = (4/\pi) \times Q_{sn}\ \text{Exp}[-0.148\ t] \times W_s/(E\ C_p)\ (\varepsilon Q_{sn} - \varepsilon E)$

$\text{Max}\ \Delta(\text{ONI}) = (4/\pi)\ 7.05 \times 10^{21} \times \text{Exp}[-0.148\ t] \times 0.0238/(1.09 \times 10^{17} \times 1\ 000) \times (0.2\text{-}0.09)$

$\text{Max}\ \Delta(\text{ONI}) = \pm 0.57 \times \text{Exp}[-0.148\ t]$

For t=1, or 1997, Max Δ(ONI)=±0.49 °C.

For t=10, or 2006, Max Δ(ONI)=±0.13 °C.

For t=18, or 2014, Max Δ(ONI)=±0.039 °C.

6. Discussion

The Oceanic Niño Index as defined and calculated by (NOAA 2023; NCAR 2023) includes variability of sources of heat exchanged in El Niño region 3.4, including but not limited to the effects of volcanic eruptions, solar cycle, global surface temperature rise, and typhoon count cycle. Figure 1 illustrates graphically in solid red lines the annual average value of the index for ENSO period between 1996 and 2015. The index appears to have carried over -0.5 °C from the previous oscillation. The dashed lines in red color are two-year moving average of the observed index. For comparison with the calculated index in blue color, the observed index should be imagined to be translated upward by 0.5 °C. At the beginning of the period, the calculated error of oscillation amplitude is ±0.49 °C, and the phase angle error is ±8.13°. The calculated and observed indexes are well within the error margins. The error in amplitude decreases

with time, and towards the middle of the period, it assumes ±0.13 °C, and the phase error approaches ±81.3°. Here too, cycle phases may coincide within the error margins; however, index values are mixed, they vary between about the same values to considerable deviation. Towards the end of the period, the amplitude error decreases to ±0.039 °C, and the phase error increases to ±146.37°. The observed phases are well within the error margins, but some amplitudes deviate. When, however, two-year moving average is considered for the observed index, the amplitudes and phase angles adhere closely to the theoretically calculated values. Some discrepancy between the observed and calculated indexes should be expected. Because the theoretical index does not include variability of heat sources; it is triggered by initial conditions that do not vary with time.

As Fig. 1 reveals, the calculated amplitude of the index decreases with time and amplitude error decreases with time as well as discussed earlier. The oscillation thus tends towards stability. Furthermore, the derived equation (20) is a sinusoidal function whose amplitude contains a decay factor, and the resulting index is asymmetric and non linear. The warm phases are expected to have larger amplitudes than the succeeding cold phases. This is in line with observations, which present ENSO models do not capture, please refer to Introduction. The damped oscillation requires energy supply, and this energy does not appear to be accounted for in the current knowledge as discussed in the introduction section. Wind thrust and momentum fluxes provide the required energy during El Niño events. The resulting air mass oscillation appears to exist: Jaramillo et al. (2021) observed a decrease in the height of tropical tropopause during El Niño episodes and an increase during La Niña episodes. Clearly, there is an observed correlation between air potential energy fluctuation and ENSO warm and cold phases.

7. Conclusions

As per the discussion section, the existence of air mass potential energy cycles during ENSO phases by Jaramillo et al. (2021) are in good agreement with the theory presented. The derived theoretical equation (20) of the index captures observed features such as index asymmetry and non linearity, which present models do not capture. Contrary to the current perception, the oscillation is not self-driven indefinitely; energy is supplied continually during El Niño events that maintain the oscillation. Equation (20) appears to yield a reasonable agreement between the theoretical and observed values of the oceanic Niño indexes within error margins and average index variability. The equation may thus fill a void in the current ENSO understanding, and may potentially represent ENSO climatology. Major error contributors are El Niño area, A_n, and evaporation, E, in Niño region, both of which are unavailable with accuracy at this time.

The entire work is based on the concept that the difference in sea temperature between the hemispheres has produced heat cycles in the hydrosphere in the form of warm water that culminates with El Niño events. These in turn provide continual energy supply that maintains ENSO. Sea temperature difference between the northern and southern hemispheres is presently increasing based on data available (CRU 2023). Temperature projection may follow T_{SH}-T_{NH}=-0.01 x-0.052 for the near future, where x is line number of Table 1. Accordingly, El Niño is expected to occur more frequently. Using the same calculation methodology, ENSO is calculated and projected for the period between 2015 and 2024, Fig 4 in blue color.

The projection has an accuracy of ±1 year for the entire period. Adjustment for sea temperature variation due to volcanic eruptions, solar cycle, global sea temperature rise, and typhoon count cycle may be necessary.

Finally, there is room for improvement. The scale selection of one year has been chosen to eliminate seasonal variability. The derived Eq. (20) may well be used on monthly and quarterly scales. In these cases, seasonal variability of poleward heat transport and seasonal temperature variation must be accounted for with the motion of the earth around the sun. Calculations using shorter scales require computer simulation of the mass and heat balance of the hemispheres for every scale selected. And errors of ENSO parameter such as evaporation, El Niño heat, El Niño area, and others should be minimized.

Declarations

8. Acknowledgements

The author acknowledges that this manuscript is entirely authentic and genuine and the entire work has been prepared by the author. This manuscript is not currently being considered for publication by other journals. No data has been fabricated or manipulated. Furthermore, the author declares no conflicts of interest with respect to the research, authorship, and publication of this manuscript. This publication is funded by the Author.

10. Funding

This publication is funded by the author

11. Competing Interests

The author declares no conflicts of interest with respect to the research, authorship, and publication of this manuscript.

12. Author contributions

The author prepared the entire work including text, tables, and figures.

13. Data availability statements

Anomalies of sea surface temperature are available online at https://crudata.uea.ac.uk/cru/data/temperature/, Temperature, Temperature data (HadCRUT4, CRUTEM4) climate research, under tab “Data for downloading and file formats,” HadSST4, Version 4.0.1.0”, University of East Anglia, Climate Research Unit, Norwich, U. K. The observed Oceanic Nino index is available online at National Oceanic and Atmospheric Administration website, Climate Prediction Center-ONI-NOAA, Cold & Warm Episodes by Season, https://www.origin.cpc.necp.noaa.gov/products/analysis_monitoring/ensostuff/ONI_v5.php

References

An IS, Jin FF (2004) Nonlinearity and Asymmetry of ENSO. Journal of Climate 17, 2, 2399-2412. https://doi.org/10.1175/1520-0442(2004)017<2399:NAAOE>2.0.CO;2

Caballero R (2014) Physics of the Atmosphere. IOP Publishing Ltd, Bristol, U. K., pp. 2-1 to2-33, 3-1 to 3-29, 6-1 to 6-5.

Caviedes CN (2001) El Niño in history storming through the ages. University Press of Florida, Gainesville, Florida, U.S.A., 279 p.

Chanduvi-acña F (1969) A study of Evaporation and Evapotranspiration in Peru. All Graduate Thesis and Dissertations. 1555, Utah State University. https://digitalcommons.usu.edu/cgi/viewcontent.cgi?article=2554&context=etd

CRU (2023) Temperature, Temperature data (HadCRUT4, CRUTEM4) climate research, under tab “Data for downloading and file formats,” HadSST4, Version 4.0.1.0”, University of East Anglia, Climate Research Unit, Norwich, U. K. https://crudata.uea.ac.uk/cru/data/temperature/

(Website accessed October, 1, 2023).

Fleagle RG, Businger JA (1980) An Introduction to Atmospheric Physics, 2nd edn, Van Mieghem J, Hales AL (Eds.), Academic Press, New York, 432 p., pp. 4-20, 52, 151-176, 415.

Goldberg N (1996) Air Conditioning, Heating, and Ventilation, In: Avallone EA, Baumeisterm T. III (Eds.), Mark's Standard Handbook for Mechanical Engineers, 10th ed., McGraw-Hill, New York, pp. 12-86.

Gruber A, Levizzani V (2008) Assessment of Global Precipitation Products, World Climate Research Program, Global Energy and Water Cycle. Geneva, Switzerland: World Meteorological Organization, WCRP-128, WMO/TD-No. 1430.

Hayashi M, Jin FF, Stuecker MF (2020) Dynamics for El Niño-La Niña asymmetry constrains equatorial-Pacific warming pattern. Nat Commun 11, 4230 (2020). doi:/10.1038/s41467-020-17983-y

Jaramillo A, Dominguez C, Raga G, Quintanar AI (2021) The combined QBO and ENSO Influence on Tropical Cyclone Activity over the North Atlantic Ocean. Atmosphere 2021, 12(12), 1588. https://doi.org/10.3390/atmos12121588

Koltzbach PJ (2011) El Niño-Southern Oscillation's Impact on Atlantic Basin Hurricanes and U.S. Landfalls. Journal of Climate 24, 1252-1263. Https://doi.org/10.1175/2010JCL13799.1

Lau KM, Yang S (2015) Tropical Meteorology & Climate Walker Circulation, In: Pyle GR, North J, Zhang F (Eds.), Encyclopedia of Atmospheric Physics, 2nd edn., Elsevier, Amsterdam, Netherland.

Li J, Xie S, Cook E et al. (2011) Interdecadal modulation of El Niño amplitude during the past millennium. Nature Climate Change 1, 114-118. https://doi.org/10.1038/nclimate1086

Lin KH, Van Ness HC, Abbott MM (1984) Thermodynamics, In: Crawford HB, Eckes BE (Eds.), Perry's Chemical Engineers Handbook, 6th edn, Mc Graw-Hill, New York, pp. 4-52, 4-59.

NCAR (2023) Climate Data (Nino 1+2, 3, 3.4, 4; ONI and TNI), National Center for Atmospheric Research, Boulder, CO, U.S.A. https://climatedataguide.ucar.edu (Website accessed October 15, 2023).

NOAA (2023) Description of Changes to Ocean Niño Index, Climate Prediction Center-ONI-NOAA, Cold & Warm Episodes by Season, Centered 30-year base period, National Oceanic and Atmospheric Administration, Manchester, MA, U.S.A. https://www.origin.cpc.necp.noaa.gov/products/analysis_monitoring/ensostuff/ONI_v5.php. (Website accessed on October, 5, 2023).

NOAA (2022) El Ninio/Southern Oscillation, Equatorial Pacific Sea Temperature. National Oceanic and Atmospheric Administration, Manchester, MA, U.S.A. https://www.neci.noaa.gov. (Website accessed on December, 5, 2022).

Swedan N (2020) Parameterization of energy cycles between the hemispheres. Science Progress 103: issue 2. https://doi.org/10.1177/0036850420922773

Swedan NH (2018) Calculation of Open Water Evaporation as a Climate Parameter. Journal of Water Resource and Protection 10, 762-779. https://doi.org/10.4236/jwarp.2018.108043

Trenberth KE, Caron JM, Stepaniak DP et al. (2002) Evolution of El Niño–Southern Oscillation and global atmospheric surface temperatures. Journal of Geophysical Research 107: no. d8. https://doi.org/10.1029/2000JD000298

Trenberth KE, Hoar TJ (1996) The 1990-1995 El Niño Southern Oscillation event: Largest on record. Geophysical Research Letters 23 (1), 57-60. https://doi.org/10.1029/95GL03602

Wang C (2018) A review of ENSO theories. National Science Review 5, 813–825. doi: 10.1093/nsr/nwy104

Wang C, Deser C, Yu JY et al. (2016) El Niño-Southern Oscillation (ENSO): A review, In: Glymn P, Manzello D, Enochs I (Eds.), Coral Reefs of the Eastern Pacific, Springer Science Publisher, Dordrecht, 85-106. doi: 10.1007/978-94-017-7499-4_4

Ward PJ, Kummu M, Lall U. (2016) Flood frequencies and durations and their response to El Niño Southern Oscillation: Global analysis. Journal of Hydrology 529, 358-378, https://doi.org/10.1016/j.jhydrol.2016.05.045

Symbols And Abbreviations

A_n	Surface area of El Niño event, m^2
β	Volumetric thermal expansion of sea water, $°C^{-1}$
C_p	Specific heat of air mixture, J kg^{-1} $°C^{-1}$
d	A symbols that denotes an infinitesimal variation
ε	Relative error of measurement or calculated parameter
Δ	A symbol that denotes a small variation or absolute error in measurement or calculation
d^{-1}	Per day
d_m	Average depth of ocean mixed layer, m
δ	Average air density of the lower atmosphere, kg m^{-3}
$δ_n$	Average air density in El Niño region, kg m^{-3}
E	Evaporation in El Niño region before and after El Niño event, kg yr^{-1}
ENSO period	Time in years between two consecutive El Niño event
E_n	Evaporation in El Niño region during El Niño event, kg s^{-1}
Exp (x)	Exponential function of natural logarithm base, equal to e^x
F_z	Component of the resultant of atmospheric force in Z direction, N.
F_b	Force of air buoyancy, N
Fc	Force of Coriolis, N
g	Gravity acceleration, m s^{-2}
m	Mass of air between sea level and tropical tropopause in El Niño region,
	Kg
M_n	Air mass flow rate in El Niño region during El Niño event, kg s^{-1}
M	Air mass flow rate in El Niño region before and after El Niño event, kg s^{-1}
n	Number of years between two consecutive El Niño events, years.
N	Newton
ONI	Oceanic Niño Index, °C

P	Pressure of the atmosphere, kPa
Q_a	Heat gained by an arbitrary air mass, J kg^{-1}
Q_s	Heat removed from the surface by an arbitrary air mass, J kg^{-1}
ΔQ_n	Annual heat accumulation in El Niño region, J
Q_{PHT}	Poleward heat transport, 5.52×10^{22} J yr^{-1}
Q_{sn}	Cumulative annual heat in El Niño region in n years, J
$Q_s(t)$	Heat anomaly of sea water in El Niño region, J
s	Second
t	Time in years
τ	Earth's revolution time around the sun, 3.15×10^7 s
T_{NH}	Average sea temperature of the northern hemisphere, °C
T_{SH}	Average sea temperature of the southern hemisphere, °C
T_{sn}	Sea temperature in El Niño region, °C
U	Internal energy of an arbitrary air parcel, J
V	Volume of air mass, m^3
v	Vertical component of air velocity in El Niño region, m s^{-1}
v_h	Horizontal component of air velocity in El Niño region, m s^{-1}
v_n	Vertical component of air velocity in El Niño region during El Niño event, m s^{-1}
V_r	Relative velocity between air mass in El Niño region and surface, m s^{-1}
W	Work produced by an arbitrary air mass, J kg^{-1}
W_s	Air humidity at saturation, kg water per kg dry air
W_t	Air humidity at tropical tropopause, 0 kg water per kg dry air
ω	Angular velocity of the earth around its rotation axis, radians s^{-1}
yr	Year
Z	Vertical coordinate, height above sea level, m
ξ	Fluctuation in the height of tropopause Z_T or air mass above sea water, m

Tables

Table 1. Calculation of El Niño heat Q_{sn} for the period of time between 1997 and 2015 in which two consecutive El Niño events occurred. NH is abbreviation of northern hemisphere, SH is abbreviation of southern hemisphere. Data source is CRU (2023).

Line No.	Year	Temperature anomaly NH, ˚C	Temperature anomaly SH, ˚C	T_{SH}-T_{NH} ˚C	Cumulative Heat, J
1	1997	---	---	---	0.00E+00
2	1998	0.540	0.479	-0.061	1.60E+20
3	1999	0.306	0.247	-0.059	3.15E+20
4	2000	0.329	0.231	-0.098	5.73E+20
5	2001	0.430	0.354	-0.076	7.72E+20
6	2002	0.460	0.41	-0.050	9.04E+20
7	2003	0.536	0.385	-0.151	1.30E+21
8	2004	0.550	0.331	-0.219	1.88E+21
9	2005	0.557	0.345	-0.212	2.44E+21
10	2006	0.517	0.338	-0.179	2.91E+21
11	2007	0.461	0.266	-0.195	3.42E+21
12	2008	0.435	0.241	-0.194	3.93E+21
13	2009	0.520	0.442	-0.078	4.14E+21
14	2010	0.557	0.422	-0.135	4.49E+21
15	2011	0.417	0.342	-0.075	4.69E+21
16	2012	0.527	0.376	-0.151	5.09E+21
17	2013	0.555	0.389	-0.166	5.52E+21
18	2014	0.713	0.442	-0.271	6.24E+21
19	2015	0.861	0.553	-0.308	7.05E+21

Figures

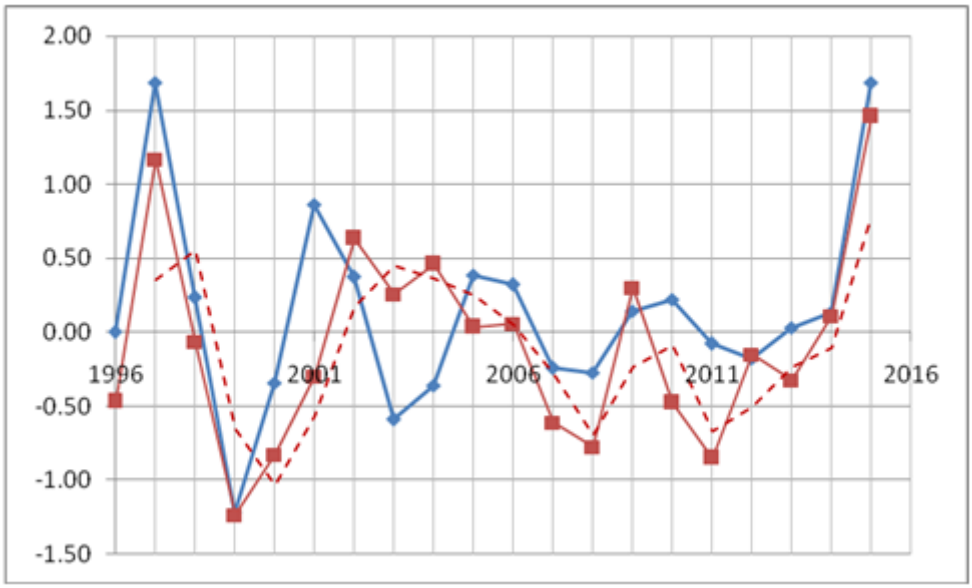

Figure 1

The observed (solid red lines) and calculated (blue color) of the average value of the Oceanic NiñoIndex, Niño region 3.4, in degrees C for the period of time between 1996 and 2015. The dashed line in red color is two-year moving average of the observed index. The data source of the observed index is National Oceanic and Atmospheric Administration (NOAA 2023).

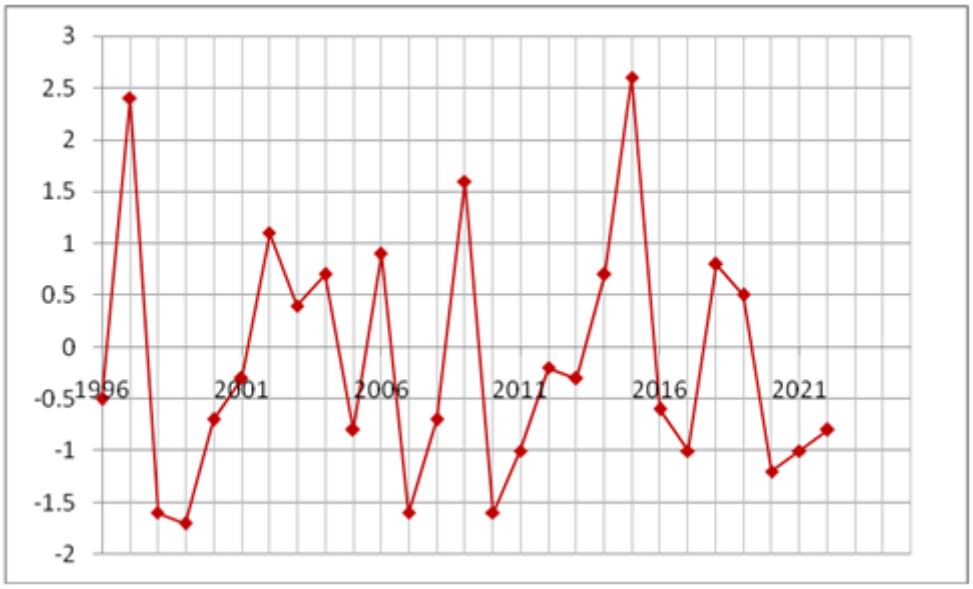

Figure 2

The observed average value of the Oceanic Niño Index, Niño region 3.4, in degrees C for the months of November, December, and January. These are the months when El Niño events typically occur. Data source is National Oceanic and Atmospheric Administration (NOAA 2023).

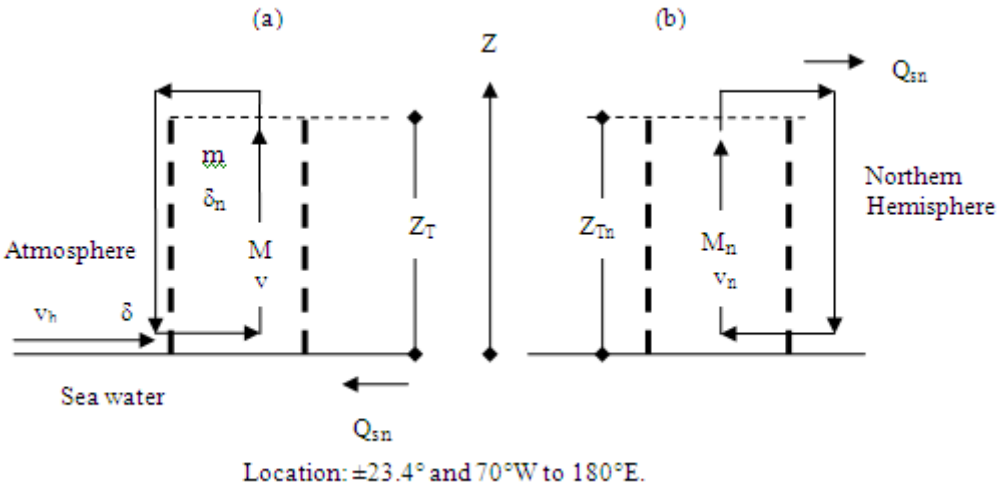

Figure 3

Heat transfer, air mass flow, and air volume of the lower atmosphere in El Niño region enclosed by the dashed lines. (a) Before and after El Niño event. (b) During El Niño event. M=Vertical component of the

tropical air flow before and after El Niño event, kg s^{-1}; v=Vertical velocity component of tropical winds in Z direction, m s^{-1}; v_h=Horizontal velocity component of tropical winds, m s^{-1}; Z_T=Height of tropical tropopause, m; Z_{Tn}=Height of tropical tropopause during El Niño event, m; Q_{sn}=Solar heat of El Niño, J; M_n=Vertical air mass flow during El Niño event, kg s^{-1}; v_n=Vertical air velocity in Z direction during El Niño event, m s^{-1}.

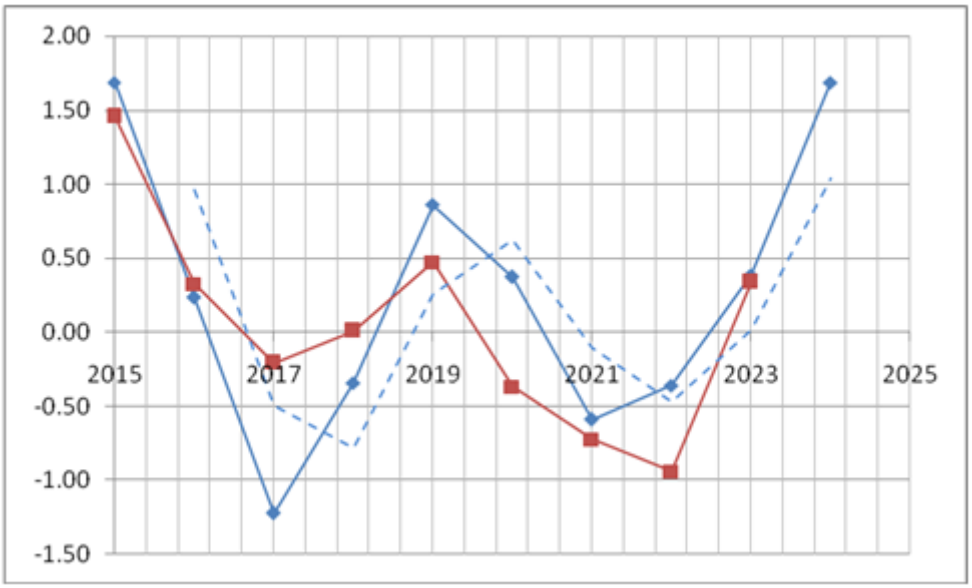

Figure 4

The calculated and projected average Oceanic Niño Index, Niño region 3.4, in degrees °C for the period of time between 2015 and 2024 (solid blue lines). The lines in red color are the observed annual average value of the index. The dashed blue lines are two-year moving average of the calculated index. The observed data source is National Oceanic and Atmospheric Administration (NOAA, 2023) through August 2023.